THE ASTROPHYSICAL JOURNAL, 413:811–825, 1993 August 20

ENERGY TRANSPORT TO THE SOLAR CORONA BY MAGNETIC KINK WAVES

ARNAB RAI CHOUDHURI,[1] MAUSUMI DIKPATI,[1,2] AND DIPANKAR BANERJEE[2]
Received 1992 October 19; accepted 1993 January 29

ABSTRACT

We show that the magnetic kink waves generated by the motions of photospheric footpoints of the coronal flux tubes can supply adequate energy for heating the quiet corona, provided there are occasional rapid motions of these footpoints as found in recent observations (Vigneau et al. 1992). Choudhuri, Auffret, & Priest (1992) modeled the solar corona as isothermal atmosphere and showed that these rapid motions are much more efficient for transporting energy compared to the slow footpoint motions taking place most of the time. We extend these calculations for a two-layer atmosphere, with the lower layer having chromospheric thickness and temperature, and the upper layer having coronal temperature. Even in the presence of such a temperature jump, we find that the rapid footpoint motions are still much more efficient for transporting energy to the corona and the estimated energy flux is sufficient for quiet coronal heating, i.e., we reinforce the conclusions of Choudhuri, Auffret, & Priest (1992).

In addition to presenting results for the solar corona, we discuss the general problem of the propagation of kink pulses in a two-layer atmosphere for different possible values of the basic parameters. We find a fairly complicated behavior which could not be anticipated from the analysis of a pure Fourier mode. For pulses generated by rapid footpoint motions, the energy flux decreases due to reflection at the transition layer. For pulses generated by slow footpoint motions, however, the behavior of the system is governed by modes, which are evanescent in the lower layer, but can tunnel through it. The energy flux carried by such pulses can actually increase when there is a temperature jump in the atmosphere.

Subject headings: MHD — Sun: corona

1. INTRODUCTION

Two mechanisms have been suggested for heating the solar corona—direct dissipation of magnetic topologies and dissipation of waves (Parker 1986; Hollweg 1990; Ulmschneider, Priest, & Rosner 1991; Narain & Ulmschneider 1991). Though it is conceivable that both these mechanisms are operative in the closed active region loops, the heating of the quiet corona with open magnetic field lines can only be due to the dissipation of hydromagnetic waves which are produced by photospheric disturbances and then propagate along magnetic field lines. The magnetic flux at the photospheric level exists as isolated flux tubes, which fan out upward and eventually merge with each other above the chromosphere. Hence the waves carrying energy from the photosphere to the corona can be modeled, at least in the layers just above the photosphere, as waves propagating along magnetic flux tubes. A question of crucial importance is: what is the nature of these waves? If thin flux tube equations are used to study the wave propagation along flux tubes, then one obtains two kinds of solutions corresponding to the sausage and kink modes (Spruit 1981; Roberts 1985). By using the full MHD equations, one can show the existence of a third kind of mode—the shear Alfvén mode (also called torsional Alfvén mode)—which cannot be handled by thin flux tube equations (Hollweg 1990). Most probably the movements of flux tube footpoints give rise to a mixture of all these modes (see discussion and figure in § 2 of Hollweg 1981).

Some recent observations suggest that the flux tube footpoints occasionally undergo rapid motions for short durations (Vigneau et al. 1992). The theoretical implications of these rapid intermittent motions have been studied by Choudhuri, Auffret, & Priest (1992, hereafter Paper I). Since the observations are discussed in detail in Paper I, we do not discuss them here. It was pointed out in Paper I that such jerky motions of footpoints would give rise to kink modes in the flux tubes above, and the properties of these kink modes were studied by considering an isothermal atmosphere of photospheric temperature above the photosphere. It was found that these occasional jerky motions were much more efficient for sending energy to the corona compared to the slow Brownian motions of footpoints that must be taking place most of the time. A calculation of the energy flux using the isothermal atmosphere model and incorporating these rapid footpoint motions suggested a value of energy flux well above what is needed for heating the quiet corona. In the actual solar atmosphere, however, one may expect the flux to be reduced due to reflections from the transition layer where the temperature jumps sharply from chromospheric to coronal values. The aim of this paper is to extend the calculations of Paper I for a two-layer atmosphere, which illustrates how the energy transport to the corona is influenced by the temperature jump in the transition layer.

The reflection of the shear Alfvén mode (i.e., torsional Alfvén mode) at the transition layer has been studied by several authors (Hollweg 1981, 1984; Zugzda & Locans 1982). One may at first expect that the reflection of kink modes will be of very similar nature. A qualitative difference between the two situations, however, arises from the fact that the kink modes propagating along flux tubes in a gravitationally stratified atmosphere have a cutoff frequency below which they do not propagate, whereas there is no such lower cutoff for the shear Alfvén mode. Most wave modes in gravitationally stratified atmospheres—starting from the simplest

[1] Department of Physics, Indian Institute of Science, Bangalore-560012, India.
[2] Indian Institute of Astrophysics, Bangalore-560034, India.

acoustic mode (Lamb 1932)—have cutoff frequencies. The shear Alfvén mode is one very special mode which does not couple to gravity, at least in the linear theory with purely horizontal displacements, and hence does not have a cutoff frequency. We show that the reflection of kink modes having frequencies close to the gravitational cutoff frequency is a much more subtle and much richer problem than the problem of reflections of the shear Alfvén mode without a cutoff.

Let us consider a vertical thin flux tube embedded in a two-layer atmosphere, the lower layer of height h having a temperature T_1 and the upper layer having a higher temperature T_2 (i.e., $T_2 > T_1$). Such a two-layer model, on the one hand, is not a bad model for the solar atmosphere (see Fontenla, Avrett, & Loeser 1990) and has been used by many authors. On the other hand, it has the virtue of being sufficiently simple so that one can understand the basic physics by studying how various results change on varying the basic parameters. The cutoff frequency ω_{c_2} of hot upper layer will be less than that of the lower layer (i.e., $\omega_{c_2} < \omega_{c_1}$). For frequencies larger than ω_{c_1}, the modes will propagate in both the layers. On the other hand, modes with frequencies less than ω_{c_2} will be evanescent in both the layers. But for the intermediate frequencies between ω_{c_2} and ω_{c_1}, the modes will be evanescent in the lower layer and propagating in the upper layer. If the lower layer extended over many scale heights, then these intermediate modes would not be able to take away any energy flux. On the other hand, if the lower layer were sufficiently thin, then these modes can "tunnel" through it and then propagate in the upper layer. Hence, under certain circumstances, the asymptotic energy flux, instead of becoming less than what it would have been in an isothermal atmosphere with temperature T_1, actually becomes more if there is a temperature jump from T_1 to T_2 with a hotter layer above! Something like this is never possible for a mode like the shear Alfvén mode without a cutoff, for which, if there is a jump to higher temperature in the overlying atmosphere, the flux is always reduced due to reflection compared to the flux in the isothermal atmosphere. Most previous studies of this mode involved the study of a particular Fourier component, and this was sufficient to understand the behavior of the mode. However, for kink modes behaving very differently in different frequency ranges, it is not sufficient to look at individual Fourier components in order to understand the basic physics. Hence we study the propagation in this two-layer atmosphere of kink pulses having wide ranges of frequencies in their spectral resolution.

A previous study of kink propagation along flux tubes in the solar atmosphere was reported by Spruit (1984) in a conference proceedings with the words: "I present here briefly the results from a model calculation for the propagation and excitation of transversal waves (to be published in more detail elsewhere)." However, a more detailed account has not appeared after that. Though our calculations are in the same spirit, we concentrate on several aspects of the problem not discussed by Spruit (1984). It may be noted that Spruit (1984) incorporated the merging of flux tubes above a certain height. Since our analytical expressions for pulse propagation become quite formidable even without the merger of flux tubes, we have not incorporated it in this paper, though we wish to look at the effects of merger in future. The emphasis in this paper has been to understand the basic physics of pulse propagation along isolated flux tubes in the presence of a temperature jump without putting other additional complications.

Much of the paper is devoted to studying the basic physics of the problem. We present a fairly exhaustive parameter space study to illustrate the nature of kink wave propagation in a two-layer atmosphere for different possible combinations of the basic parameters. Finally at the end, we apply our general results to the solar atmosphere. We reinforce the main conclusion of Paper I that the rapid footpoint motions are much more efficient for transporting energy to the corona. Even in the presence of the temperature jump at the transition layer, the rapid footpoint motions are able to transmit sufficient energy to heat the quiet corona, though the energy flux is somewhat reduced due to reflection from the transition layer. For the slow footpoint motions, on the other hand, the energy flux may increase slightly due to the "tunneling" effect described above.

The next section studies the nature of a Fourier component of the kink mode in a two-layer atmosphere. Then § 3 discusses how the Fourier modes can be superposed to provide a kink pulse. The parameter space study is presented in § 4. We apply our results to the solar atmosphere in § 5. Finally the last section summarizes our conclusions.

2. THE NATURE OF A FOURIER MODE

We consider the propagation of a kink mode of frequency ω along a vertical flux tube in a two-layer atmosphere. The lower layer with temperature T_1 is taken to extend from $z = 0$ to $z = h$, and the upper layer with temperature T_2 starts from $z = h$. The pressure scale heights in the two layers are proportional to the temperatures, i.e., the ratio of the temperatures is the same as the ratio of the scale heights. We list the two assumptions used throughout the paper.

1. The flux tube along which the kink propagates is considered isolated, i.e., we do not take into account the merging of neighboring flux tubes above the photospheric level.
2. We neglect nonlinear effects so that any kink disturbance can be represented by a linear superposition of individual Fourier modes.

The kink mode coming from below reaches the interface $z = h$, where a part of the wave gets reflected downward into the first layer and the rest transmits into the second layer. The solution for a kink mode in an isothermal atmosphere was presented in equations (32)–(34) of Spruit (1981). Using this solution, we write the velocity in the first layer as the linear combination of an upward propagating wave and a downward propagating reflected wave, whereas the velocity in the second layer consists of only the upward propagating transmitted wave:

$$v_1(z, t) = \{\hat{v}_u(\omega) \exp [i\omega t - ik_1(\omega)z] + \hat{v}_d(\omega) \exp [i\omega t + ik_1(\omega)z]\} \exp (z/4H_1) , \quad (1a)$$

$$v_2(z, t) = \hat{v}_t(\omega) \exp [i\omega t - ik_2(\omega)z] \exp (z/4H_2) , \quad (1b)$$

where $\hat{v}_u(\omega)$, $\hat{v}_d(\omega)$, $\hat{v}_t(\omega)$ represent the amplitudes of the original wave, reflected wave, and transmitted wave respectively, whereas H_1

and H_2 are the pressure scale heights. The wavenumbers $k_1(\omega)$ and $k_2(\omega)$ are related to ω as follows (Spruit 1981):

$$k_1(\omega) = \pm \frac{1}{4H_1}\left(\frac{\omega^2}{\omega_{c_1}^2} - 1\right)^{1/2}, \tag{2a}$$

$$k_2(\omega) = \pm \frac{1}{4H_2}\left(\frac{\omega^2}{\omega_{c_2}^2} - 1\right)^{1/2}, \tag{2b}$$

where ω_{c_1} and ω_{c_2} are the cutoff frequencies of the first and second layers given by

$$\omega_{c_1}^2 = \frac{g}{8H_1}\frac{1}{2\beta + 1}, \tag{3a}$$

and

$$\omega_{c_2}^2 = \frac{g}{8H_2}\frac{1}{2\beta + 1}. \tag{3b}$$

If we assume the flux tubes to be in thermal equilibrium with the surroundings, it can be easily shown that $\beta = 8\pi p/B^2$ has to be a constant inside a particular layer. The continuity of pressure and magnetic field across the interface further ensures that β is continuous across the interface, i.e., it is constant everywhere. We now relate $\hat{v}_u(\omega)$, $\hat{v}_d(\omega)$, and $\hat{v}_t(\omega)$ by using the boundary conditions to be satisfied across the interface $z = h$. Firstly, the displacements on the two sides have to be matched. From equations (1a) and (1b), the corresponding displacements in the two layers can be written as

$$\xi_1(z, t) = \frac{1}{i\omega}\{\hat{v}_u(\omega)\exp[i\omega t - ik_1(\omega)z] + \hat{v}_d(\omega)\exp[i\omega t + ik_1(\omega)z]\}\exp\left(\frac{z}{4H_1}\right), \tag{4}$$

$$\xi_2(z, t) = \frac{1}{i\omega}\{\hat{v}_t(\omega)\exp[i\omega t - ik_2(\omega)z]\}\exp\left(\frac{z}{4H_2}\right). \tag{5}$$

By matching these expressions of displacements at the interface at $z = h$, we have

$$\hat{v}_u(\omega)\exp\left[-ik_1(\omega)h + \frac{h}{4H_1}\right] + \hat{v}_d(\omega)\exp\left[ik_1(\omega)h + \frac{h}{4H_1}\right] = \hat{v}_t(\omega)\exp\left[-ik_2(\omega)h + \frac{h}{4H_2}\right]. \tag{6}$$

The secondary boundary condition can be obtained from the basic equation of kink mode propagation (eq. [31] in Spruit 1981), which is

$$(2\beta + 1)\partial_{tt}\xi = g\,\partial_z\xi + \beta v_A^2\,\partial_{zz}\xi. \tag{7}$$

By integrating this equation from $z = h - \epsilon$ to $z = h + \epsilon$ (ϵ being a very small quantity), it is easily seen that

$$\partial_z\xi\Big|_{h-\epsilon} = \partial_z\xi\Big|_{h+\epsilon}, \tag{8}$$

i.e., $\partial_z\xi$ has to be continuous across $z = h$.

Applying equation (8), we have

$$\left[-ik_1(\omega) + \frac{1}{4H_1}\right]\hat{v}_u(\omega)\exp\left[-ik_1(\omega)h + \frac{h}{4H_1}\right] + \left[ik_1(\omega) + \frac{1}{4H_1}\right]\hat{v}_d(\omega)\exp\left[ik_1(\omega)h + \frac{h}{4H_1}\right]$$
$$= \left[-ik_2(\omega) + \frac{1}{4H_2}\right]\hat{v}_t(\omega)\exp\left[-ik_2(\omega)h + \frac{h}{4H_2}\right]. \tag{9}$$

From equations (6) and (9),

$$\hat{v}_d(\omega) = \frac{\{i[k_1(\omega) - k_2(\omega)] - [(1/4H_1) - (1/4H_2)]\}\exp[-2ik_1(\omega)h]}{\{i[k_1(\omega) + k_2(\omega)] + [(1/4H_1) - (1/4H_2)]\}}\hat{v}_u(\omega), \tag{10}$$

$$\hat{v}_t(\omega) = \frac{2ik_1(\omega)\exp\{-i[k_1(\omega) - k_2(\omega)]h + h[(1/4H_1) - (1/4H_2)]\}}{\{i[k_1(\omega) + k_2(\omega)] + [(1/4H_1) - (1/4H_2)]\}}\hat{v}_u(\omega). \tag{11}$$

Thus the amplitudes of reflected and transmitted waves are expressed in terms of the incident upward wave so that the amplitude of the incident wave, which is a measure of the overall amplitude, remains the only free parameter.

In order to study the transmission of energy toward the corona in this two-layer model, we define the transmission coefficient $\mathcal{T}$ as the ratio of the energy density due to the transmitted wave at the bottom of the second layer to the energy density due to the original wave at the footpoint:

$$\mathcal{T} = \frac{\rho_2(h)A_2(h)v_2^2(h)}{\rho_{1,0}A_{1,0}v_u^2(0)}, \tag{12}$$

where ρ's and A's are densities and cross sectional areas of the flux tube in the two layers as given by

$$\rho_1(z) = \rho_{1,0} \exp(-z/H_1), \tag{13a}$$

$$\rho_2(z) = \rho_{2,0} \exp(-z/H_2), \tag{13b}$$

$$A_1(z) = A_{1,0} \exp(z/2H_1), \tag{14a}$$

$$A_2(z) = A_{2,0} \exp(z/2H_2), \tag{14b}$$

and v_u is the part of v_1 as given in equation (1a) which corresponds to the upward wave. The quantities $\rho_{1,0}$, $\rho_{2,0}$, $A_{1,0}$, $A_{2,0}$ are related to one another in the following way. Since the pressure is continuous across $z = h$,

$$\rho_1(h)T_1 = \rho_2(h)T_2,$$

or

$$\rho_{2,0} = \frac{T_1}{T_2}\rho_{1,0} \exp\left(-\frac{h}{H_1} + \frac{h}{H_2}\right). \tag{15}$$

Again since the flux tube must be continuous at $z = h$,

$$A_1(h) = A_2(h),$$

or

$$A_{2,0} = A_{1,0} \exp\left(\frac{h}{2H_1} - \frac{h}{2H_2}\right). \tag{16}$$

Using equations (1), (11), (13), (14), (15), and (16), we can write the expression (12) as

$$\mathcal{T} = \frac{T_1}{T_2}\left|\frac{2ik_1(\omega)\exp[-ik_1(\omega)h]}{i[k_1(\omega)+k_2(\omega)] + [(1/4H_1) - (1/4H_2)]}\right|^2. \tag{17}$$

It is to be noted that we are defining the transmission coefficient $\mathcal{T}$ as a ratio of energy densities, whereas the more usual practice is to define it as a ratio of energy fluxes. Our motivation behind using densities rather than fluxes is to develop a uniform approach which would be applicable even in the cases where the wave in the lower layer is evanescent and there is no flux in that layer. We can express $\mathcal{T}$ as a function of frequencies by using the dispersion relations for the two layers given in equations (2a) and (2b). From equations (3a) and (3b) it can easily be seen that the cutoff frequency ω_{c_1} of the first layer is higher than the cutoff frequency ω_{c_2} of the hotter second layer and

$$\omega_{c_2}/\omega_{c_1} = \sqrt{T_1/T_2}. \tag{18}$$

Choosing the signs of $k_1(\omega)$ and $k_2(\omega)$ in such a way that the propagating waves propagate upward and the evanescent waves die away with height, we have the following five combinations of $k_1(\omega)$ and $k_2(\omega)$ for different ranges of ω.

$$\text{For } -\infty < \omega < -\omega_{c_1}, \begin{cases} k_1(\omega) = -\dfrac{1}{4H_1}\left(\dfrac{\omega^2}{\omega_{c_1}^2} - 1\right)^{1/2}, \\ k_2(\omega) = -\dfrac{1}{4H_2}\left(\dfrac{\omega^2}{\omega_{c_2}^2} - 1\right)^{1/2}, \end{cases} \tag{19a}$$

$$\text{for } -\omega_{c_1} < \omega < -\omega_{c_2}, \begin{cases} k_1(\omega) = -\dfrac{i}{4H_1}\left(1 - \dfrac{\omega^2}{\omega_{c_1}^2}\right)^{1/2}, \\ k_2(\omega) = -\dfrac{1}{4H_2}\left(\dfrac{\omega^2}{\omega_{c_2}^2} - 1\right)^{1/2}, \end{cases} \tag{19b}$$

$$\text{for } -\omega_{c_2} < \omega < \omega_{c_2}, \begin{cases} k_1(\omega) = -\dfrac{i}{4H_1}\left(1 - \dfrac{\omega^2}{\omega_{c_1}^2}\right)^{1/2}, \\ k_2(\omega) = -\dfrac{i}{4H_2}\left(1 - \dfrac{\omega^2}{\omega_{c_2}^2}\right)^{1/2}, \end{cases} \tag{19c}$$

$$\text{for } \omega_{c_2} < \omega < \omega_{c_1}, \begin{cases} k_1(\omega) = -\dfrac{i}{4H_1}\left(1 - \dfrac{\omega^2}{\omega_{c_1}^2}\right)^{1/2}, \\ k_2(\omega) = \dfrac{1}{4H_2}\left(\dfrac{\omega^2}{\omega_{c_2}^2} - 1\right)^{1/2}, \end{cases} \tag{19d}$$

$$\text{for } \omega_{c_1} < \omega < \infty, \begin{cases} k_1(\omega) = \dfrac{1}{4H_1}\left(\dfrac{\omega^2}{\omega_{c_1}^2} - 1\right)^{1/2}, \\ k_2(\omega) = \dfrac{1}{4H_2}\left(\dfrac{\omega^2}{\omega_{c_2}^2} - 1\right)^{1/2}. \end{cases} \tag{19e}$$

The transmission coefficient $\mathcal{T}$ for any frequency can now be found out by substituting the appropriate combination for $k_1(\omega)$ and $k_2(\omega)$ in equation (17).

At this point, it is useful to introduce a set of dimensionless variables, some of which have already been introduced in Paper I. Here we shall make the variables dimensionless with respect to the constants of the first layer.

$$u = \frac{\omega}{\omega_{c_1}}, \tag{20}$$

$$\tau = \omega_{c_1} t, \tag{21}$$

$$s = \frac{z}{4H_1}, \tag{22}$$

$$\alpha = \frac{h}{4H_1}, \tag{23}$$

$$r^2 = \frac{T_1}{T_2}, \tag{24}$$

so that

$$\omega_{c_2}/\omega_{c_1} = r. \tag{25}$$

Here u, τ, and s are dimensionless frequency, time, and height, respectively, which were already used in Paper I. The other two variables α and r are the two basic parameters for the two layer atmosphere. They are, respectively, measures of the thickness of the lower layer and the temperature contrast between the two layers.

It is easy to see from equation (17) that $\mathcal{T}$ is symmetric in positive and negative frequencies. Hence we write down the expressions of $\mathcal{T}$ for different ranges of positive frequencies only. Choosing the proper expressions from equations (19a)–(19e), for $u < r$, i.e., when the waves are evanescent in both the layers, we have

$$\mathcal{T} = \frac{4r^2(1-u^2)\exp\left(-2\alpha\sqrt{1-u^2}\right)}{\left[\sqrt{1-u^2} + r\sqrt{r^2-u^2} + (1-r^2)\right]^2}. \tag{26a}$$

For $r < u < 1$, i.e., when the waves are evanescent in the first layer but propagating in the second layer,

$$\mathcal{T} = \frac{4r^2(1-u^2)\exp\left(-2\alpha\sqrt{1-u^2}\right)}{r^2(u^2-r^2) + \left[\sqrt{1-u^2} + (1-r^2)\right]^2}. \tag{26b}$$

For $u > 1$, i.e., when the waves are propagating in both the layers,

$$\mathcal{T} = \frac{4r^2(u^2-1)}{\left(\sqrt{u^2-1} + r\sqrt{u^2-r^2}\right)^2 + (r^2-1)^2}. \tag{26c}$$

By varying the values of r and α, we can study how the transmission of energy changes when the temperature ratio of the two layers is changed or the height of the interface is altered.

In Figures 1*a* and 1*b*, $\mathcal{T}$ has been plotted against frequency u. Figure 1*a* shows the transmission for different values of r, smaller r corresponding to larger temperature contrasts between the layers. For $u > 1$, the mode is propagating in both the layers and we expect the transmission of energy to decrease as the temperature jump increases to produce larger reflection. We see in Figure 1*a* that $\mathcal{T}$ is reduced for smaller r not only when $u > 1$ but also when $u < 1$. If we have the frequency in the range $r > u > 1$, then the mode can propagate in the upper layer after tunneling through the lower. With larger temperature jump (i.e., smaller r), the range of tunneling becomes larger. Hence, though the value of $\mathcal{T}$ is smaller for smaller r, the overall energy transport may enhance with smaller r because of this increase in the range of tunneling. We shall actually show in the next section that the transmission of a low-frequency pulse can become more efficient in a two-layer atmosphere if the upper layer is made hotter, thereby making r smaller and increasing the range of tunneling. Figure 1*b* shows how $\mathcal{T}$ changes on changing α for a particular r. When the mode is propagating in both layers (i.e., $u > 1$), $\mathcal{T}$ is independent of α as can be seen in equation (26c). Only when the mode is evanescent in the lower layer, $\mathcal{T}$ decreases with increasing α (which is a measure of the thickness of the lower layer).

3. PULSE PROPAGATION

After considering a Fourier component of the kink mode in the last section, we now study the propagation of a pulse along the flux tube which can be represented as a superposition of the Fourier components. As in Paper I, we consider a pulse generated by a footpoint motion having a Gaussian profile of velocity as a function of time:

$$v_x(z = 0, t) = v_0 e^{-bt^2}. \tag{27}$$

The total displacement due to this motion is finite and given by

$$L = \sqrt{\frac{\pi}{b}}\, v_0. \tag{28}$$

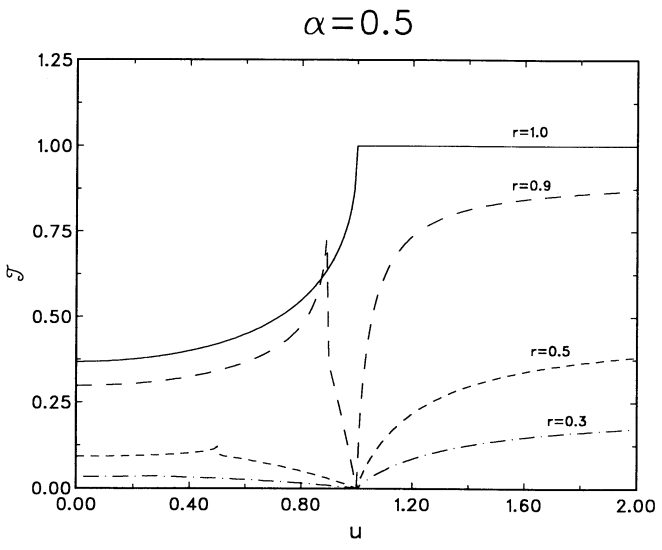

FIG. 1a

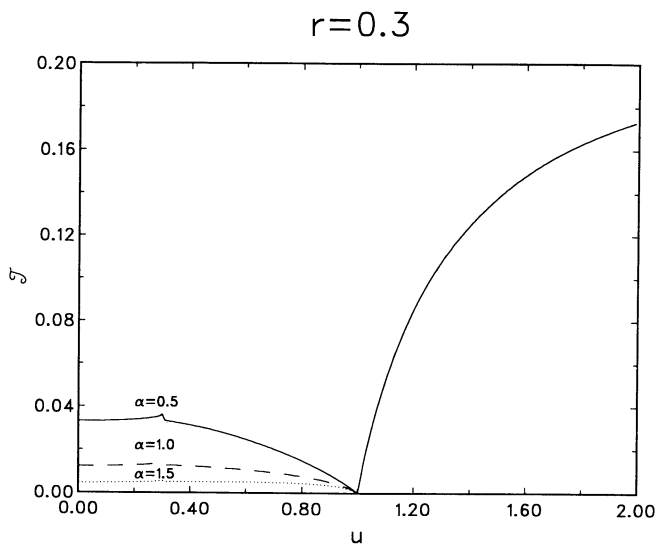

FIG. 1b

FIG. 1.—(*a*) Transmission coefficient $\mathcal{T}$ as a function of frequency $u(=\omega/\omega_{c_1})$ for different temperature contrasts $r(=\sqrt{T_1/T_2})$ and a fixed thickness $\alpha(=h/4H_1)=0.5$ of the first layer. (*b*) Transmission coefficient $\mathcal{T}$ as a function of frequency $u(=\omega/\omega_{c_1})$ for different α (i.e., thickness of the first layer) for a particular temperature contrast $r=0.3$.

Though the velocity is mathematically nonzero at all times, it is appreciable only from time $-1/b^{1/2}$ to time $+1/b^{1/2}$. Hence a finite motion of the footpoint in finite time can roughly be modeled with such a Gaussian profile. To find the response of the flux tube to such a motion, we superpose the Fourier modes as given in equation (1), i.e.,

$$v_1(z,t)=\int_{-\infty}^{+\infty}\{\hat{v}_u(\omega)\exp[i\omega t-ik_1(\omega)z]+\hat{v}_d(\omega)\exp[i\omega t+ik_1(\omega)z]\}\exp\left(\frac{z}{4H_1}\right)d\omega\,, \tag{29a}$$

$$v_2(z,t)=\int_{-\infty}^{+\infty}\hat{v}_t(\omega)\exp[i\omega t-ik_2(\omega)z]\exp\left(\frac{z}{4H_2}\right)d\omega\,. \tag{29b}$$

The corresponding displacements of the flux tubes in the two layers are

$$\xi_1(z,t)=\int_{-\infty}^{+\infty}\frac{d\omega}{i\omega}\{\hat{v}_u(\omega)\exp[i\omega t-ik_1(\omega)z]+\hat{v}_d(\omega)\exp[i\omega t+ik_1(\omega)z]\}\exp\left(\frac{z}{4H_1}\right), \tag{30a}$$

$$\xi_2(z,t)=\int_{-\infty}^{+\infty}\frac{d\omega}{i\omega}\{\hat{v}_t(\omega)\exp[i\omega t-ik_2(\omega)z]\}\exp\left(\frac{z}{4H_2}\right). \tag{30b}$$

Since we have already related $\hat{v}_d(\omega)$ and $\hat{v}_t(\omega)$ to $\hat{v}_u(\omega)$ in equations (10) and (11), we just have to find out $\hat{v}_u(\omega)$ from the footpoint motion equation (27). Using equations (10), (27), and (29a), we have

$$\hat{v}_u(\omega)=\frac{\{i(k_1+k_2)+[(1/4H_1)-(1/4H_2)]\}e^{ik_1h}}{ik_1(e^{ik_1h}+e^{-ik_1h})+ik_2(e^{ik_1h}-e^{-ik_1h})+[(1/4H_1)-(1/4H_2)](e^{ik_1h}-e^{ik_1h})}\frac{v_0}{2\sqrt{\pi b}}e^{-(u\omega^2/4b)}\,. \tag{31}$$

We now introduce one more dimensionless variable in addition to the ones introduced earlier:

$$\lambda=\frac{v_0}{\omega_{c_1}L}\,. \tag{32}$$

where λ is a parameter which gives the strength of the jerking at the footpoint. It was already defined and used in Paper I. Substituting equations (10), (11), and (31) in equations (30a), (30b) and using the dimensionless variables as given in equations (20), (21), (22), (23), (25), and (32), and also recalling the dispersion relations for different ranges of ω as given in the expression (19a)–(19e), we find after some extensive but straightforward algebra that

$$\xi_1(s,\tau)=\frac{L}{\pi}\left\{\int_0^r du\,e^{[s-(u^2/4\pi\lambda^2)]}\frac{\chi_i\cosh[(s-\alpha)\chi_i]-(r^2\chi_i'+q)\sinh[(s-\alpha)\chi_i]}{\chi_i\cosh(\alpha\chi_i)+(r^2\chi_i'+q)\sinh(\alpha\chi_i)}\frac{\sin(u\tau)}{u}\right.$$
$$\left.+\int_r^1 du\,e^{[s-(u^2/4\pi\lambda^2)]}\frac{\chi_i q\sinh[(2\alpha-s)\chi_i]+\chi_i^2\cosh(\alpha\chi_i)\cosh[(s-\alpha)\chi_i]}{[r^2\chi_r'\sinh(\alpha\chi_i)]^2+[\chi_i\cosh(\alpha\chi_i)+q\sinh(\alpha\chi_i)]^2}\frac{\sin(u\tau)}{u}\right.$$

$$
\begin{aligned}
&- \int_r^1 du\, e^{[s-(u^2/4\pi\lambda^2)]} \frac{(r^4\chi_r'^2 + q^2)\sinh(\alpha\chi_i)\sinh[(s-\alpha)\chi_i]}{[r^2\chi_r'\sinh(\alpha\chi_i)]^2 + [\chi_i\cosh(\alpha\chi_i) + q\sinh(\alpha\chi_i)]^2} \frac{\sin(u\tau)}{u} \\
&- \int_r^1 du\, e^{[s-(u^2/4\pi\lambda^2)]} \frac{r^2\chi_i\chi_r'\sinh(s\chi_i)}{[r^2\chi_r'\sinh(\alpha\chi_i)]^2 + [\chi_i\cosh(\alpha\chi_i) + q\sinh(\alpha\chi_i)]^2} \frac{\cos(u\tau)}{u} \\
&+ \int_1^\infty du\, e^{[s-(u^2/4\pi\lambda^2)]} \frac{\chi_r q\sin[(2\alpha - s)\chi_r] + \chi_r^2\cos(\alpha\chi_r)\cos[(s-\alpha)\chi_r]}{r^4\chi_r'^2\sin^2(\alpha\chi_r) + [\chi_r\cos(\alpha\chi_r) + q\sin(\alpha\chi_r)]^2} \frac{\sin(u\tau)}{u} \\
&- \int_1^\infty du\, e^{[s-(u^2/4\pi\lambda^2)]} \frac{(r^4\chi_r'^2 + q^2)\sin(\alpha\chi_r)\sin[(s-\alpha)\chi_r]}{r^4\chi_r'^2\sin^2(\alpha\chi_r) + [\chi_r\cos(\alpha\chi_r) + q\sin(\alpha\chi_r)]^2} \frac{\sin(u\tau)}{u} \\
&- \int_1^\infty du\, e^{[s-(u^2/4\pi\lambda^2)]} \frac{r^2\chi_r\chi_r'\sin(s\chi_r)}{r^4\chi_r'^2\sin^2(\alpha\chi_r) + [\chi_r\cos(\alpha\chi_r) + q\sin(\alpha\chi_r)]^2} \frac{\cos(u\tau)}{u}\Bigg\}, \qquad (33a)
\end{aligned}
$$

$$
\begin{aligned}
\xi_2(s,\tau) = \frac{L}{\pi}\Bigg\{ &\int_0^r du\, e^{[\alpha+y-y\chi_i'-(u^2/4\pi\lambda^2)]} \frac{\chi_i}{\chi_i\cosh(\alpha\chi_i) + (r^2\chi_i' + q)\sinh(\alpha\chi_i)} \frac{\sin(u\tau)}{u} \\
&+ \int_r^1 du\, e^{[\alpha+y-(u^2/4\pi\lambda^2)]} \frac{\chi_i[\chi_i\cosh(\alpha\chi_i) + q\sinh(\alpha\chi_i)]}{r^4\chi_r'^2\sinh^2(\alpha\chi_i) + [\chi_i\cosh(\alpha\chi_i) + q\sinh(\alpha\chi_i)]^2} \frac{\sin(u\tau - y\chi_r')}{u} \\
&- \int_r^1 du\, e^{[\alpha+y-(u^2/4\pi\lambda^2)]} \frac{r^2\chi_i\chi_r'\sinh(\alpha\chi_i)}{r^4\chi_r'^2\sinh^2(\alpha\chi_i) + [\chi_i\cosh(\alpha\chi_i) + q\sinh(\alpha\chi_i)]^2} \frac{\cos(u\tau - y\chi_r')}{u} \\
&+ \int_1^\infty du\, e^{[\alpha+y-(u^2/4\pi\lambda^2)]} \frac{\chi_r[\chi_r\cos(\alpha\chi_r) + q\sin(\alpha\chi_r)]}{r^4\chi_r'^2\sin^2(\alpha\chi_r) + [\chi_r\cos(\alpha\chi_r) + q\sin(\alpha\chi_r)]^2} \frac{\sin(u\tau - y\chi_r')}{u} \\
&- \int_1^\infty du\, e^{[\alpha+y-(u^2/4\pi\lambda^2)]} \frac{r^2\chi_r\chi_r'\sin(\alpha\chi_r)}{r^4\chi_r'^2\sin^2(\alpha\chi_r) + [\chi_r\cos(\alpha\chi_r) + q\sin(\alpha\chi_r)]^2} \frac{\cos(u\tau - y\chi_r')}{u}\Bigg\}, \qquad (33b)
\end{aligned}
$$

where

$$\chi_i = \sqrt{1-u^2}\,, \qquad (34a)$$

$$\chi_i' = \sqrt{1-u^2/r^2}\,, \qquad (34b)$$

$$\chi_r = \sqrt{u^2-1}\,, \qquad (34c)$$

$$\chi_r' = \sqrt{u^2/r^2-1}\,, \qquad (34d)$$

$$y = r^2(s-\alpha)\,, \qquad (34e)$$

$$q = 1 - r^2\,. \qquad (34f)$$

To calculate the displacements, we evaluate the integrals numerically. For $\alpha = 0.5$ and $r = 0.3$, the displacements have been plotted versus altitude for different times in Figures 2*a* and 2*b*. As in Paper I, here also we find that for slow footpoint motion (i.e., $\lambda = 0.2$), the flux tubes always remain close to vertical while being shifted. For stronger footpoint motion (i.e., $\lambda = 1.0$), the disturbance is found to propagate as a kink pulse and the flux tube oscillates for some time before relaxing. Whenever a pulse propagates through a stratified medium, it is known to leave a wake behind it oscillating with the cutoff frequency of the atmosphere (Lamb 1932; Rae and Roberts 1982). For a single layer solar atmosphere model, Paper I clearly shows the evidence of a wake oscillating with the cutoff frequency. In our two-layer model, however, the situation is somewhat more complicated, since each layer has its own characteristic cutoff frequency. Figures 3*a*, 3*b*, and 3*c* show wakes for three different combinations of α and λ. From Figure 3*a*, we find that for not too large λ and α, the wake mainly oscillates with the cutoff frequency of the upper layer, which corresponds for $r = 0.3$ to a period of 6π in our dimensionless units. A careful look at Figure 3*a*, however, reveals the existence of another frequency with a very low amplitude. The amplitude of this frequency grows with increasing λ (i.e., stronger footpoint motion) as in Figure 3*c* or with increasing α (i.e., thicker lower layer) as in Figure 3*b*. This new frequency is neither the cutoff of the lower layer nor that of the upper layer. It has a value somewhat, though not very, close to $\omega_{c_1} + \omega_{c_2}$, which corresponds to a period 1.54π. Presumably this frequency is due to the coupling between the two layers and becomes more prominent as the effect of the lower layer becomes more dominant.

We now discuss how to find out the energy transmitted to the corona. The expression for energy per unit length of the flux tube at a particular altitude at an instant of time (using dimensionless units) is

$$\mathscr{E}(s,\tau) = \tfrac{1}{2}\rho_1(s)A_1(s)\dot{\xi}_1^2(s,\tau)\omega_{c_1}^2 \quad \text{for} \quad s \le \alpha\,, \qquad (35a)$$

$$= \tfrac{1}{2}\rho_2(s)A_2(s)\dot{\xi}_2^2(s,\tau)\omega_{c_1}^2 \quad \text{for} \quad s > \alpha\,, \qquad (35b)$$

where the dot represents differentiation with respect to $\tau = \omega_{c_1}t$. We can easily find $\dot{\xi}_1(s,\tau)$ and $\dot{\xi}_2(s,\tau)$ by differentiating the expressions (33a) and (33b). The expressions for $\rho_1(s)$, $\rho_2(s)$, $A_1(s)$, $A_2(s)$ are obtained from equations (13a)–(14b) on substituting

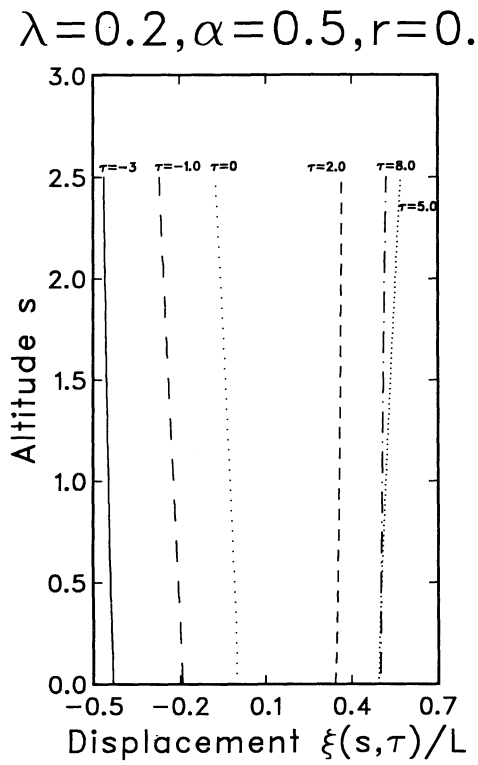

FIG. 2a

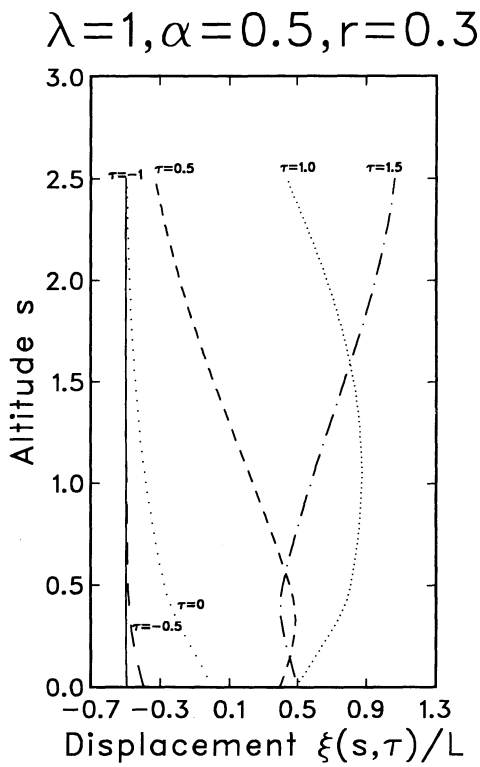

FIG. 2b

FIG. 2.—Displacement ξ (in units of the total displacement L) of the magnetic flux tube as a function of altitude $s(=z/4H_1)$ at various instants $\tau(=\omega_{c_1}t)$ for (*a*) $\lambda = 0.2$ and (*b*) $\lambda = 1.0$.

$4H_1 s$ for z. We evaluate $\mathscr{E}(s, \tau)$ numerically and plot it against the altitude s for three values of τ in Figure 4 (taking $r = 0.3$, $\alpha = 1.0$, $\lambda = 1.0$). When τ is small, the energy has not propagated much and we find the maximum of it is residing in the first layer. But after a while, when it reaches the second layer, suddenly its speed of propagation increases as a result of the larger group velocity $d\omega/dk$ in the upper layer, whereas its amplitude falls due to the jump to lower density. Hence we find that the amplitude of the energy density suddenly drops in the upper layer, though the energy propagates more quickly to the higher altitude so that the energy conservation is not violated.

To find out the total kinetic energy $\mathscr{E}_{\rm tot}(\tau)$ residing in the whole flux tube, we integrate $\mathscr{E}(s, \tau)$ from $s = 0$ to $s = \infty$, which gives

$$\mathscr{E}_{\rm tot}(\tau) = \frac{4\rho_{1,0} A_{1,0} v_{1,0}^2 H_1}{\lambda^2} F(\lambda, \alpha, r, \tau) , \tag{36}$$

where

$$\begin{aligned} F(\lambda, \alpha, r, \tau) = \frac{1}{2\pi^2} \int_0^\alpha ds \Bigg\{ \int_0^r du\, e^{-(u^2/4\pi\lambda^2)} \cos(u\tau) \frac{\chi_i \cosh[(s-\alpha)\chi_i]}{\chi_i \cosh(\alpha\chi_i) + (r^2\chi_i' + q)\sinh(\alpha\chi_i)} \\ - \int_0^r du\, e^{-(u^2/4\pi\lambda^2)} \cos(u\tau) \frac{(r^2\chi_i' + q)\sinh[(s-\alpha)\chi_i]}{\chi_i \cosh(\alpha\chi_i) + (r^2\chi_i' + q)\sinh(\alpha\chi_i)} \\ + \int_r^1 du\, e^{-(u^2/4\pi\lambda^2)} \cos(u\tau) \frac{\chi_i q \sinh[(2\alpha - s)\chi_i] - \chi_i^2 \cosh(\alpha\chi_i)\cosh[(s-\alpha)\chi_i]}{(\chi_i \cosh\alpha\chi_i + q \sinh\alpha\chi_i)^2 + r^4\chi_r'^2 \sinh^2(\alpha\chi_i)} \\ - \int_r^1 du\, e^{-(u^2/4\pi\lambda^2)} \cos(u\tau) \frac{(r^4\chi_r'^2 + q^2)\sinh(\alpha\chi_i)\sinh[(s-\alpha)\chi_i]}{[\chi_i \cosh(\alpha\chi_i) + q\sinh(\alpha\chi_i)]^2 + [r^2\chi_r' \sinh(\alpha\chi_i)]^2} \\ + \int_r^1 du\, e^{-(u^2/4\pi\lambda^2)} \sin(u\tau) \frac{r^2\chi_i\chi_r' \sinh(s\chi_i)}{[\chi_i \cosh(\alpha\chi_i) + q\sinh(\alpha\chi_i)]^2 + [r^2\chi_r' \sinh(\alpha\chi_i)]^2} \\ + \int_1^\infty du\, e^{-(u^2/4\pi\lambda^2)} \cos(u\tau) \frac{\chi_r q \sin[(s-2\alpha)\chi_r] + \chi_r^2 \cos(\alpha\chi_r)\cos[(s-\alpha)\chi_r]}{r^4\chi_r'^2 \sin^2(\alpha\chi_r) + [\chi_r \cos(\alpha\chi_r) + q\sin(\alpha\chi_r)]^2} \\ - \int_1^\infty du\, e^{-(u^2/4\pi\lambda^2)} \cos(u\tau) \frac{(r^4\chi_r'^2 + q^2)\sin(\alpha\chi_r)\sin[(s-\alpha)\chi_r]}{[\chi_r \cos(\alpha\chi_r) + q\sin(\alpha\chi_r)]^2 + [r^2\chi_r' \sin(\alpha\chi_r)]^2} \end{aligned}$$

$$+\int_1^{+\infty} du\, e^{-(u^2/4\pi\lambda^2)} \sin(u\tau)\, \frac{r^2\chi_r\chi_r' \sin(s\chi_r)}{r^4\chi_r'^2 \sin^2(\alpha\chi_r) + [\chi_r \cos(\alpha\chi_r) + q \sin(\alpha\chi_r)]^2}\Bigg\}^2$$

$$+\frac{1}{2\pi^2}\int_\alpha^\infty ds \left\{\int_0^r du\, \frac{e^{[-y\chi_i' - (u^2/4\pi\lambda^2)]}\chi_i \cos(u\tau)}{\chi_i \cosh(\alpha\chi_i) + (r^2\chi_i' + q)\sinh(\alpha\chi_i)}\right.$$

$$+\int_r^1 du\, e^{-(u^2/4\pi\lambda^2)}\, \frac{\chi_i[\chi_i \cosh(\alpha\chi_i) + q \sinh(\alpha\chi_i)] \cos(u\tau - y\chi_r')}{r^4\chi_r'^2 \sinh^2(\alpha\chi_i) + [\chi_i \cosh(\alpha\chi_i) + q \sinh(\alpha\chi_i)]^2}$$

$$+\int_r^1 du\, e^{-(u^2/4\pi\lambda^2)}\, \frac{r^2\chi_i\chi_r' \sinh(\alpha\chi_i) \sin(u\tau - y\chi_r')}{r^4\chi_r'^2 \sinh^2(\alpha\chi_i) + [\chi_i \cosh(\alpha\chi_i) + q \sinh(\alpha\chi_i)]^2}$$

$$+\int_1^{+\infty} du\, e^{-(u^2/4\pi\lambda^2)}\, \frac{\chi_r[\chi_r \cos(\alpha\chi_r) + q \sin(\alpha\chi_r)] \cos(u\tau - y\chi_r')}{r^4\chi_r'^2 \sin^2(\alpha\chi_r) + [\chi_r \cos(\alpha\chi_r) + q \sin(\alpha\chi_r)]^2}$$

$$+\int_1^{\infty} du\, e^{-(u^2/4\pi\lambda^2)}\, \frac{r^2\chi_r\chi_r' \sin(\alpha\chi_r) \sin(u\tau - y\chi_r')}{r^4\chi_r'^2 \sin^2(\alpha\chi_r) + [\chi_r \cos(\alpha\chi_r) + q \sin(\alpha\chi_r)]^2}\Bigg\}^2 . \quad (37)$$

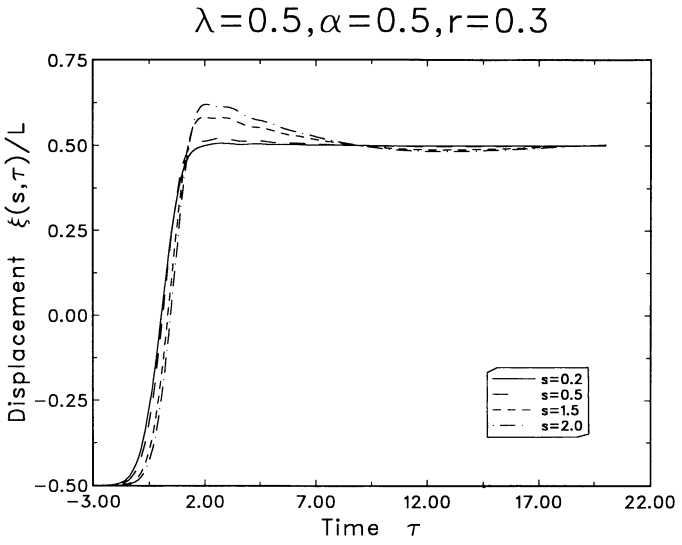

FIG. 3a

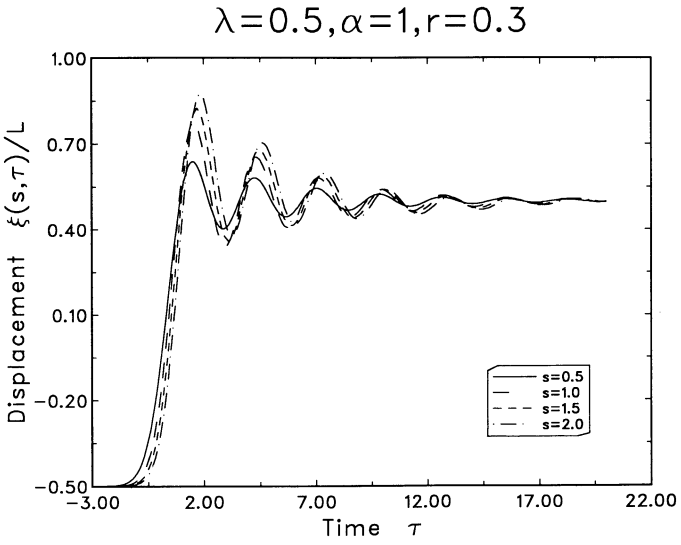

FIG. 3b

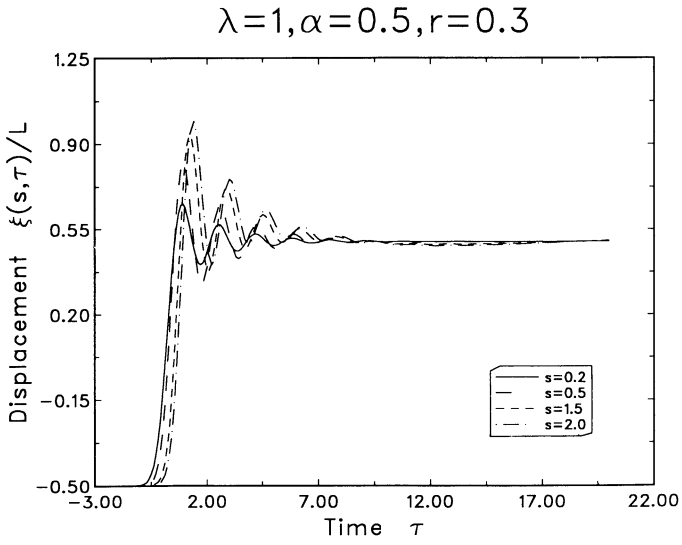

FIG. 3c

FIG. 3.—Displacement ξ of the magnetic flux tube as a function of time τ at various altitudes s for (*a*) $\lambda = 0.5$, $\alpha = 0.5$, $r = 0.3$; (*b*) $\lambda = 0.5$, $\alpha = 1.0$, $r = 0.3$; and (*c*) $\lambda = 1.0$, $\alpha = 0.5$, $r = 0.3$.

The total energy can be obtained by multiplying $\mathscr{E}_{\rm tot}(\tau)$ by

$$C = 3 + \frac{\rho_e}{\rho} + \frac{1}{\beta} \tag{38}$$

(Spruit 1981).

Though $F(\lambda, \alpha, r, \tau)$ is more complicated than the function $F(\lambda, \tau)$ introduced in Paper I, there are some resemblances. This is made clear in Figure 5, which plots $F(\lambda, \alpha = 0.5, r = 0.3, \tau)$ as a function of τ for different values of λ. This figure is strikingly similar to Figure 4 in Paper I. We again see that $F(\lambda, \alpha, r, \tau)$, which is a measure of the flux tube energy, oscillates for some time depending on whether the footpoint motion works on the flux tube or the flux tube returns the energy due to the evanescent modes to the footpoints. Eventually when the footpoint stops, $F(\lambda, \alpha, r, \tau)$ reaches a steady asymptotic value $F_{\rm asy}(\lambda, \alpha, r)$ for large τ. The energy transmitted to the corona is given by

$$\mathscr{E}_{\rm corona} = \frac{4C\rho_{1,0} A_{1,0} v_0^2 F_{\rm asy}(\lambda, \alpha, r)}{\lambda^2} . \tag{39}$$

4. PARAMETER SPACE STUDY

We have already seen in Paper I that the nature of magnetic kink pulse propagation in an isothermal atmosphere depends on the value of only one dimensionless parameter λ, which is a measure of the rapidity of the footpoint motion with respect to the cutoff frequency of the atmosphere. For the two-layer atmosphere, however, the problem becomes much richer with the introduction of two additional dimensionless parameters r and α, which are, respectively, the measures of the temperature contrast between the two layers and the thickness of the lower layer. Before choosing the values of these parameters appropriate for the solar atmosphere (done in the next section), we first study the basic physics of pulse propagation in the two-layer atmosphere by allowing the parameters to have different possible values. We, however, restrict ourselves to the study of situations in which the upper atmosphere is hotter, which implies $0 < r < 1$, since the mathematical expressions derived in the last section are valid only for this case. The temperature jump disappears if $r = 1$ and becomes more prominent as r becomes smaller. The other parameter α can lie in the range $0 < \alpha < \infty$, the limiting values of 0 and ∞ corresponding to isothermal atmospheres with temperatures T_2 and T_1, respectively. As seen in equation (37), the energy transmitted to the corona depends on all these three parameters.

Though a pulse involves the superposition of many Fourier modes, a value of λ much less than 1 means that mainly modes which are evanescent in the lower layer are present. In § 2, we have discussed the possibility of tunneling of energy to the hotter upper atmosphere even for modes evanescent in the lower layer (provided the lower layer is not too thick, i.e., α is not too large). We expect such tunneling to be noticeable mainly when λ is small. On the other hand, a larger λ implies the presence of propagating modes. For such modes, energy is reduced due to reflection and this is expected to be more important when λ is larger. Hence we may use the following rule of thumb: energy transmission at low λ is dominated by tunneling (provided α is small), whereas energy transmission at higher λ is dominated by reflection. This rule of thumb will help us a lot to make sense of the rich data we are presenting below.

For a given set of values of the three parameters λ, α, r, we numerically evaluate $F_{\rm asy}(\lambda, \alpha, r)/\lambda^2$ by using equation (37). The energy transmitted to the corona can then be easily found out by multiplying this by $4C\rho_{1,0} A_{1,0} v_0^2 H_1$, as seen in equation (39). In Figures 6*a* and 6*b*, we plot $F_{\rm asy}(\lambda, \alpha, r)/\lambda^2$ against λ for two definite values of r ($r = 0.3$ for Fig. 6*a* and $r = 0.1$ for Fig. 6*b*). In each of the

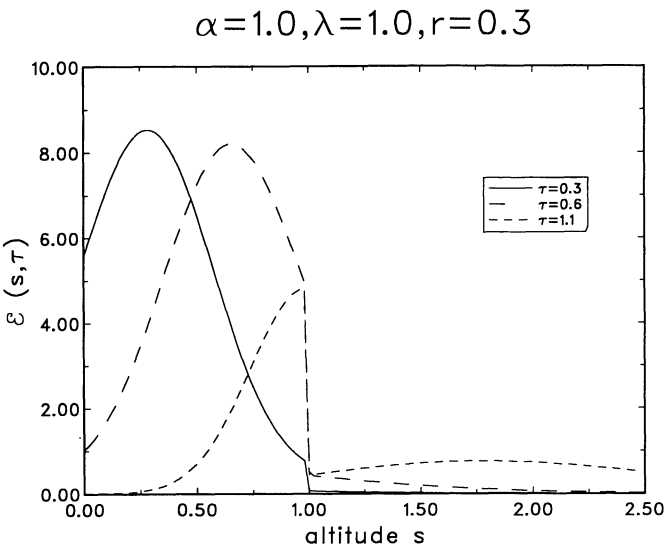

FIG. 4

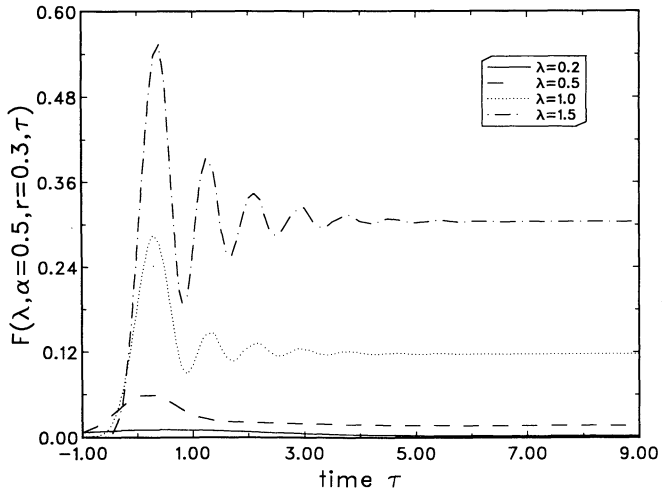

FIG. 5

FIG. 4.—Energy density $\mathscr{E}(s, \tau)$ per unit length of the flux tube as a function of altitude s at various instants τ for $\alpha = 1.0$, $\lambda = 1.0$, $r = 0.3$

FIG. 5.—Total kinetic energy $F(\lambda, \alpha, r, \tau)$ as a function of time τ for several values of λ for fixed $\alpha = 0.5$ and $r = 0.3$

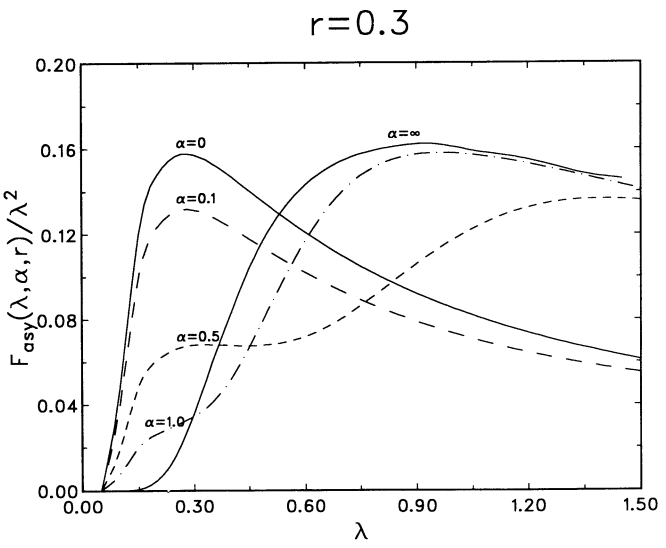

FIG. 6a

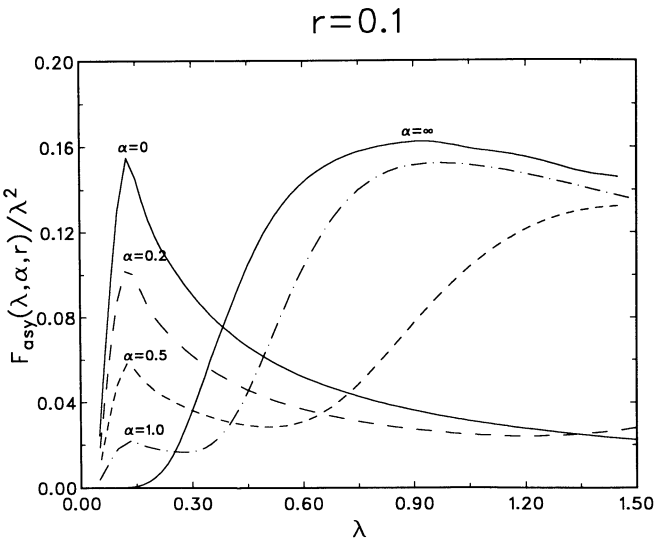

FIG. 6b

FIG. 6.—Plot of $F_{asy}(\lambda, \alpha, r)/\lambda^2$ (which is energy transmitted to the corona divided by $4C\rho_{1,0} A_{1,0} v_0^2$) as a function of λ for different α's for (*a*) $r = 0.3$, (*b*) $r = 0.1$

Figures 6*a* and 6*b*, we plot several curves corresponding to different values of α. As we have already mentioned, $\alpha = \infty$ corresponds to an isothermal atmosphere with temperature T_1. As the interface between the two layers is lowered by reducing α, the reflection becomes more important and the energy flux is initially reduced, except for very low values of λ where the tunneling becomes dominant as pointed out in our rule of thumb. This is clearly seen in Figures 6*a* and 6*b*, where we find that the energy transmission at sufficiently low λ is always enhanced by reducing α to make tunneling more efficient. When α is sufficiently small, the tunneling becomes so important that it can overcome the reflection and the flux may increase with decreasing α even for high values of λ. Finally when $\alpha = 0$, the curve corresponds to an isothermal atmosphere with temperature T_2. This curve has the same maximum value as the curve for $\alpha = \infty$ corresponding to the isothermal atmosphere with temperature T_1. In fact, it appears that one just has to shrink the curve for $\alpha = \infty$ in the horizontal direction in order to get the curve for $\alpha = 0$. We show below that this is indeed true and one can get one curve from the other by a simple scaling.

From Paper I, one can easily see that the energy transmitted to an isothermal atmosphere divided by $4C\rho_0 A_0 v_0^2 H$ is a function of $\lambda (= v_0/\omega_c L)$ alone, i.e.,

$$\frac{\mathscr{E}_{\text{corona}}(\lambda, \alpha = \infty, r)}{4C\rho_{1,0} A_{1,0} v_0^2 H_1} = G(\lambda) . \tag{40}$$

Here we have taken $\lambda = v_0/\omega_{c_1} L$. Since $\alpha = 0$ also corresponds to another isothermal atmosphere where the cutoff frequency is $\omega_{c_2} = r\omega_{c_1}$, the quantity $\mathscr{E}_{\text{corona}}(\lambda, \alpha = 0, r)/4\rho_{2,0} A_{2,0} v_0^2 H_2$ has to be the same function of $\lambda' = v_0/\omega_{c_2} L = \lambda/r$. Therefore

$$\frac{\mathscr{E}_{\text{corona}}(\lambda, \alpha = 0, r)}{4C\rho_{2,0} A_{2,0} v_0^2 H_2} = G\left(\frac{\lambda}{r}\right) = \frac{\mathscr{E}_{\text{corona}}(\lambda/r, \alpha = \infty, r)}{4C\rho_{1,0} A_{1,0} v_0^2 H_1} . \tag{41}$$

From equations (15), (16), and the fact that scale heights are proportional to temperature, it is easy to show that $\rho_{2,0} A_{2,0} H_2 = \rho_{1,0} A_{1,0} H_1$. Hence it follows from equations (39) and (41) that

$$\frac{F_{asy}(\lambda, \alpha = 0, r)}{\lambda^2} = \frac{F_{asy}(\lambda/r, \alpha = \infty, r)}{(\lambda/r)^2} . \tag{42}$$

The equation (42) clearly explains why the curve corresponding to one isothermal atmosphere is shrunk r times (as one finds in Figs. 6*a* and 6*b*) to produce the curve corresponding to another isothermal atmosphere which is $1/r^2$ times hotter. It is seen in both Figures 6*a* and 6*b* that the curves corresponding to $\alpha = \infty$ (i.e., for isothermal atmosphere with temperature T_1) have maxima at about $\lambda = 0.9$. It is clear from the scaling equation (42) that the curves for $\alpha = 0$ (i.e., for isothermal atmosphere with temperature T_2) will have maxima at $\lambda/r = 0.9$, the peak value at the maxima being the same as the peak value for the $\alpha = \infty$ curve. This is clearly borne out in Figures 6*a* and 6*b*. In fact, it will help us to understand some of the results presented below if we remember the fact that $F_{asy}(\lambda, \alpha, r)/\lambda^2$ for small values of α becomes largest when λ/r is close to 0.9.

How the reflection and the tunneling depends on the temperature contrast between the two layers becomes clear in Figure 7, in which we plot $F_{asy}(\lambda, \alpha, r)/\lambda^2$ against λ for several values of the temperature contrast (smaller r implying larger contrast), while the thickness of the lower layer is held constant ($\alpha = 0.5$). For larger λ, the effect of reflection is more dominant and the flux decreases on increasing the temperature contrast (i.e., decreasing r). For very small values of λ, on the other hand, the tunneling is more important and the flux increases as the upper layer is made hotter (by decreasing r). Thus we clearly establish the fact that the energy flux is not always diminished by reflection in the presence of a temperature jump, but the flux can actually be enhanced under certain circumstances due to the increased tunneling. This is an interesting new result which would not become apparent in a Fourier mode analysis and requires the study of pulse propagation for its derivation.

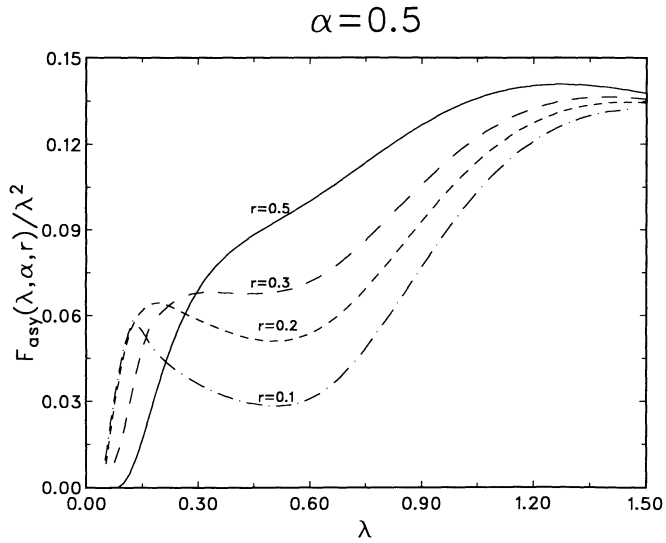

FIG. 7.—Plot of $F_{asy}(\lambda, \alpha, r)/\lambda^2$ as a function of λ for several values of temperature contrast r for a particular $\alpha = 0.5$

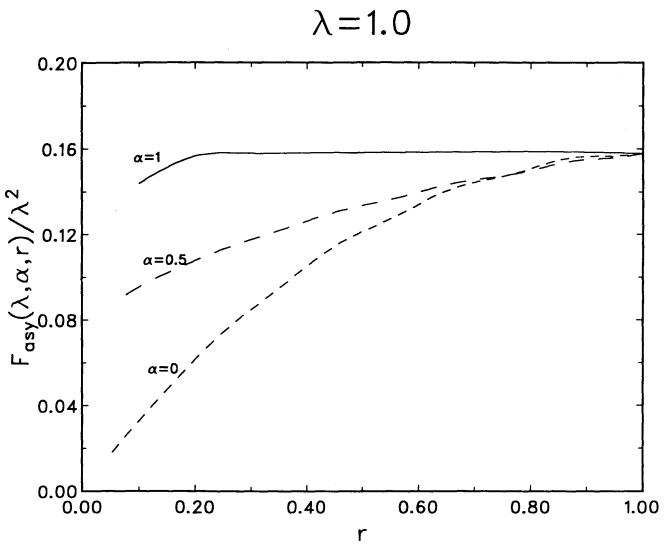

FIG. 8*a*

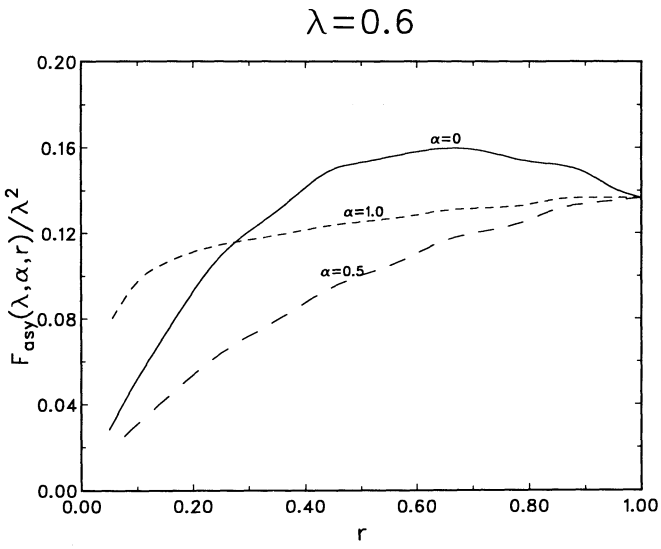

FIG. 8*b*

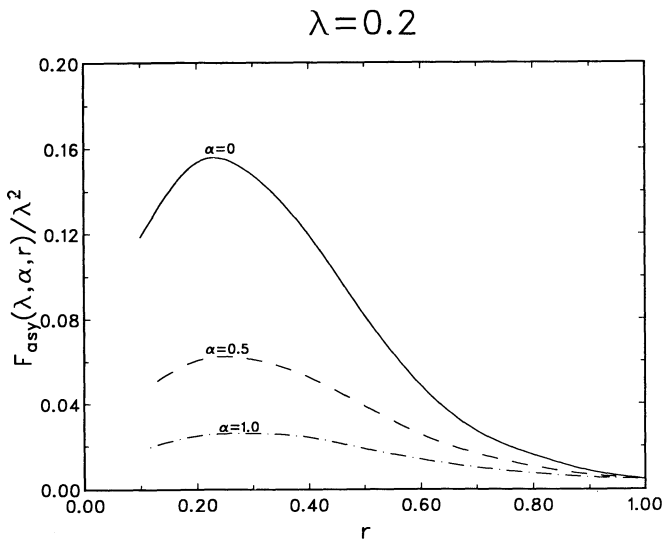

FIG. 8*c*

FIG. 8.—Plot of $F_{asy}(\lambda, \alpha, r)/\lambda^2$ as a function of temperature contrast r for different α (i.e., thickness of the first layer): (*a*) $\lambda = 1.0$, (*b*) $\lambda = 0.6$, (*c*) $\lambda = 0.2$.

Figures 8*a*, 8*b*, and 8*c* which plot $F_{asy}(\lambda, \alpha, r)/\lambda^2$ against r for three different values of λ, bring out more clearly the dependence on the temperature contrast. In Figure 8*a* with $\lambda = 1.0$, the reflection is more important and the flux decreases with larger temperature contrast (smaller r) for any value of α. On the other hand, for Figure 8*c* with $\lambda = 0.2$, we expect the tunneling to be dominant and the flux to increase with smaller r. This is seen on right-hand side of the figure. However, all the curves have maxima close to $\lambda/r = 0.9$ for reasons explained above. In Figure 8*a*, the flux is enhanced on increasing the height of the lower layer (i.e., increasing α), which makes reflection less efficient. In Figure 8*c*, however, the flux is enhanced on decreasing α, since tunneling is more important in this case. Figure 8*b* presents curves for an intermediate value of λ, for which the results are more complicated.

Finally Figures 9*a* and 9*b* show how the energy flux varies with the thickness of the lower layer. These figures present $F_{asy}(\lambda, \alpha, r)/\lambda^2$ plotted against α for two different values of λ. Figure 9*a* is for $\lambda = 1$, which makes reflection important. Unless α is very small to make tunneling important, the flux increases with height, since there is less reduction of flux due to reflection as the interface between the layers is moved higher up. The curves for higher temperature contrast (lower r) lie lower, because there is more reflection when the contrast is more. When α is sufficiently large so that hotter upper layer is far away from the footpoint, the flux becomes independent of the temperature of the upper layer and curves for different values of r coalesce. Figure 9*b* is for $\lambda = 0.2$ so that the tunneling is dominant and we find more energy to tunnel through when the height is less. The tunneling is expected to be more efficient when the upper layer is hotter (i.e., when r is smaller). Hence we may expect the curves for lower r to lie higher, which is true for $r = 0.1$ and $r = 0.5$. For $r = 0.2$ and $r = 0.3$, however, we have λ/r sufficiently close to 0.9, which makes the energy flux for these cases larger.

5. APPLICATION TO THE SOLAR ATMOSPHERE

Our task now is to calculate the energy transmitted to the corona and compare with the results of Paper I for isothermal atmosphere. The isothermal atmosphere of 6000 K temperature extending above the photosphere, which was used in Paper I, will be referred to as Model I. If one looks at the temperature-altitude curve of a standard solar atmosphere model above the photosphere (Fig. 1.2 in Priest 1982), one finds that there is a temperature jump to about 50,000 K around a height of 1500 km above the temperature minimum, and then there is another jump to temperatures of about 5×10^5 K around a height of 2000 km at the base of the low corona. The temperature plateau region between the two jumps was introduced in the earlier semiempirical models in order to account for the emission measure of the Lyman line observations (Vernazza, Avrett, & Loeser 1981). A more recent study by Fontenla et al. (1990), however, suggests that the temperature plateau is no longer needed if one includes ambipolar diffusion and hence a two-layer model is a good representation of the solar atmosphere. If we want to fit a two-layer model, perhaps the best option is to consider a hundred-fold temperature at 2000 km height. This is achieved by taking $r = 1/10$, $\alpha = 2.0$ (using the fact that the scale height near the temperature minimum is about 250 km). We refer to this as our Model II. In order to see the effect of the lower edge of the temperature plateau if it exists, we also consider a Model III with $r = \frac{1}{3}$, $\alpha = 1.5$, which corresponds to a ninefold temperature increase at a height of 1500 km.

Before presenting the results, we use equation (39) to write the expression for the asymptotic energy in a convenient form as in Paper I:

$$\mathscr{E}_{\text{corona}} = 10^{26} C \left(\frac{\rho_{1,0}}{10^{-7}\ \text{g cm}^{-3}}\right)\left(\frac{A_{1,0}}{10^5\ \text{km}^2}\right)\left(\frac{v_0}{1\ \text{km s}^{-1}}\right)^2\left(\frac{H_1}{250\ \text{km}}\right)\frac{F_{asy}(\lambda, \alpha, r)}{\lambda^2}\ \text{ergs}\ . \tag{43}$$

It has been estimated in Paper I that fast footpoint motions correspond to $\lambda = 0.44$, $v_0 = 3\ \text{km s}^{-1}$, whereas slow footpoint motions correspond to $\lambda = 0.22$, $v_0 = 1\ \text{km s}^{-1}$. Figure 10 shows a set of plots of $F_{asy}(\lambda, \alpha, r)/\lambda^2$ for the three models described above. One

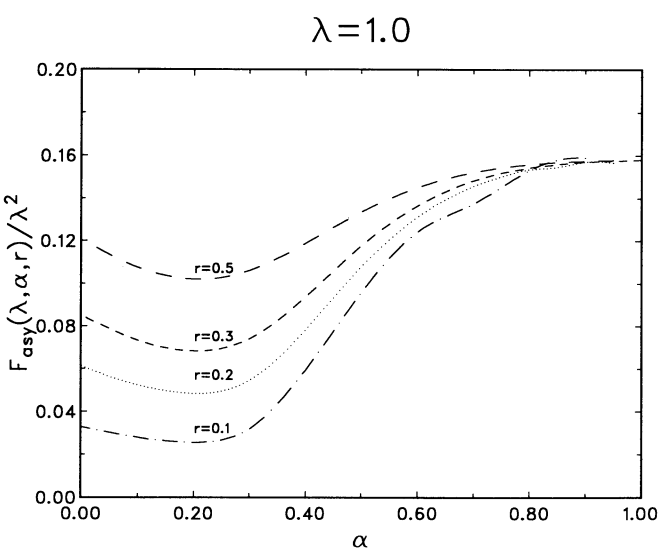

FIG. 9*a*

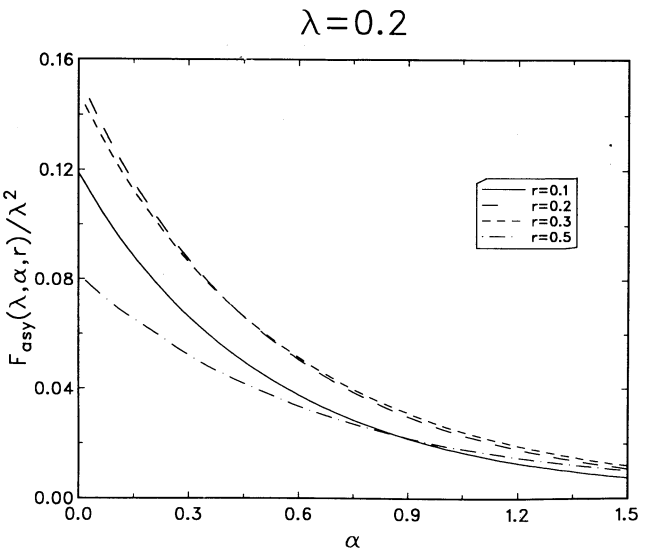

FIG. 9*b*

FIG. 9.—Plot of $F_{asy}(\lambda, \alpha, r)/\lambda^2$ as a function of α (i.e., thickness of the first layer) for several values of temperature contrast r: (*a*) $\lambda = 1.0$, (*b*) $\lambda = 0.2$

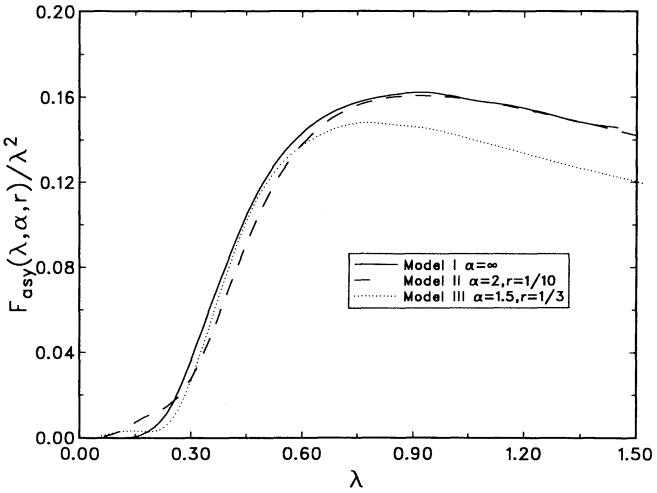

FIG. 10.—Plot of $F_{asy}(\lambda, \alpha, r)/\lambda^2$ against λ for the three models appropriate to the solar case

can now read off the value of $F_{asy}(\lambda, \alpha, r)/\lambda^2$ for a particular λ from Figure 10 and then the energy can be calculated by using equation (43). We take the density at the photospheric level $\rho_{1,0} = 3 \times 10^{-7}$ g cm^{-3}, the cross sectional area of the flux tube $A_{1,0} = 0.5 \times 10^5$ km^2 and the scale height $H_1 = 250$ km. We follow Spruit (1981) to take the constant C (defined in eq. [38]) to have a value 6.5. The values of $\mathscr{E}_{corona}$ for all the three models are given in Table 1 for both fast and slow footpoint motions.

One can finally estimate the energy flux by multiplying $\mathscr{E}_{corona}$ by the number density of footpoints and the frequency of motions. Assuming that there are about 10 footpoints in an area of 10^4 km $\times$ 10^4 km, we get a number density of 10^{-17} cm^{-2}. Since slow footpoint motions have granular time scales, we take the frequency to be about 1 in 500 s. The fast footpoint motions are less frequent and so far we do not have very reliable data on their frequency (Vigneau et al. 1992). For the purpose of rough estimate, let us take the frequency of fast motions to be once in 5000 s, i.e., 10 times infrequent compared to the slow footpoint motions. Hence the energy flux due to fast footpoint motions alone and slow footpoint motions alone can be obtained by multiplying $\mathscr{E}_{corona}$ by, respectively, 2×10^{-21} cm^{-2} s^{-1} and 2×10^{-20}. The values of energy flux for the three models are also presented in Table 1. The reader is reminded that the energy flux to heat the quiet corona is estimated to be about 3×10^5 ergs cm^{-2} s^{-1} (Hollweg 1990).

There are several things to be noted in Figure 10 and Table 1. First, the curve for Model I in Figure 10 is not very different from the other two curves. Given the other uncertainties in the model, one concludes that an isothermal atmosphere is not a bad model for the solar atmosphere as far as the propagation of magnetic kink modes are concerned. Second, the two-layer calculations reinforce the main conclusion of Paper I that the fast footpoint motions are much more important for transporting energy to the corona compared to the slow motions, even though the fast motions may be much less frequent. This is because the individual fast motions cause a much larger $\mathscr{E}_{corona}$ than the individual slow motions— both due to a larger v_0 and a larger $F_{asy}(\lambda, \alpha, r)/\lambda^2$. Hence, the contributions made by fast motions, though infrequent, is more substantial. In fact, as seen in Table 1, the energy flux due to slow footpoint motions alone for all the models falls slightly short of the requirement for heating the quiet corona. On the other hand, the rapid footpoint alone can provide the necessary energy flux. It is to be noted from Figure 10 that energy flux for rapid footpoint motions is slightly reduced in going from the isothermal model to the two-layer model, which is obviously due to reflection. But the energy flux for slow footpoint motions may get somewhat enhanced due to tunneling as we go to the two-layer model.

In summary, we identify the rapid footpoint motions as the potential source for supplying energy in the form of magnetic kink waves for heating the quiet corona. The slow motions alone would not have provided adequate energy.

6. CONCLUSION

There are two aspects of the coronal heating problem. First, we have to understand how energy is transported to the corona. Second, we have to show that the energy can be dissipated at the correct altitude. As in Paper I, here also we are concerned only with the first question of the energy transport. We point out that horizontal motions of photospheric footpoints of flux tubes would

TABLE 1

ENERGY FLUX FOR DIFFERENT CASES

	FAST MOTIONS ($\lambda = 0.44$, $v_0 = 3$ km s^{-1})		SLOW MOTIONS ($\lambda = 0.22$, $v_0 = 1$ km s^{-1})	
MODEL	$\mathscr{E}_{corona}$ (ergs)	Net Flux (ergs cm^{-2} s^{-1})	$\mathscr{E}_{corona}$ (ergs)	Net Flux (ergs cm^{-2} s^{-1})
Model I ($\alpha = \infty$)	8.75×10^{26}	1.75×10^6	9.50×10^{24}	1.90×10^5
Model II ($\alpha = 2.0, r = 1/10$)	8.35×10^{26}	1.67×10^6	6.00×10^{24}	1.20×10^5
Model III ($\alpha = 1.5, r = 1/3$)	7.90×10^{26}	1.58×10^6	1.45×10^{25}	2.90×10^5

give rise to kink waves. Though footpoint motions having granular time and velocity scales may not be sufficient for providing adequate energy, we identify the occasional rapid footpoint motions as the potential source of energy for coronal heating. As pointed out in Paper I, the slower motions dump energy mainly around the cutoff frequency, whereas the rapid footpoint motions put a substantial part of the energy above the cutoff so that the energy transport is much more efficient. Since we do not yet have sufficient data to do a proper statistical study of the rapid footpoint motions (Vigneau et al. 1992), it is difficult to make a very accurate estimate of the energy flux. A rough estimate clearly shows that the energy flux should be more than enough. Because of the importance of the rapid footpoint motions for coronal heating, more extensive observational data on such motions are urgently needed. One would also like to know how these rapid motions are produced—whether by exploding granules or by other means. We hope that future observations will clarify many of these issues.

The main thrust of this paper as compared to Paper I was to study how the propagation of the kink waves is effected by the temperature jump at the chromosphere-corona transition layer. Previous studies of wave propagation in the presence of temperature jump were done most extensively for the shear Alfvén mode (Hollweg 1981, 1984; Zugzda & Locans 1982), and it was found out the the reflection at the transition layer can reduce the energy flux substantially. These studies led to the suspicion that energy flux due to all other wave modes also may similarly be drastically reduced by reflection and not enough energy may reach the corona (Hollweg 1990). We point out that the shear Alfvén mode is somewhat special in the sense of not having a cutoff frequency and show that the propagation of kink modes having a cutoff is a very different and a richer problem. Only in the high-frequency limit (i.e., when the frequency is much larger than the cutoff frequency), the kink mode behaves similar to the shear Alfvén mode. In the solar atmosphere, however, we are in the opposite limit of the frequencies being comparable to the cutoff frequency. In this limit, the study of a pure Fourier mode does not provide adequate insight into how a pulse may propagate. Hence we have carried out calculations for pulses made up of frequencies in the different ranges. Most of the studies of the shear Alfvén mode treated only pure Fourier modes, which are good proxies for Alfvénic pulses. We have actually demonstrated cases of the energy flux being enhanced due to the presence of a temperature jump and dispelled the worry that the energy flux would always be reduced by a temperature gradient.

We have concluded that the isothermal atmosphere model used in Paper I is a fairly good model for propagation of kink pulses in the solar atmosphere. This is because of the fact that the temperature jump takes place several scale heights above the photosphere and the energy transport is not much affected by what is happening several scale heights above the footpoints, which act as drivers of the kink pulses. This is clearly seen in Figures 6*a* and 6*b*, which show that the curves for $\alpha = 1.0$ are not very different from the curves for $\alpha = \infty$. One assumption in our calculations was to neglect the merger of neighboring flux tubes above the chromosphere (Spruit 1984). However, since this merger takes place several scale heights above the photosphere, we feel that the merger also will not change the energy transport substantially, though this has to be proved by detailed calculations. We wish to look at this aspect in near future. Another assumption was to neglect the nonlinearities which must become important in the higher regions where the amplitudes are large. Nonlinear calculations for the sausage mode by Hollweg (1982) showed results very similar to the linear results of Rae & Roberts (1982), and we expect this to be true for kink modes also. We hope that more detailed simulations of kink pulse propagation in the solar atmosphere will be carried out in future by incorporating nonlinearities and by going beyond the thin flux tube approximation.

Though our calculations were done specifically for the kink mode, we believe that some of the general features we obtained will be true also for the propagation in a two-layer atmosphere of other kinds of modes having different cutoffs in the two layer. Purely acoustic waves and sausage waves on flux tubes are expected to behave very similarly. This gives us the hope our results with some modifications may be useful in other situations also, especially to the problem of wave propagation in stellar and planetary atmospheres of other types.

Mausumi Dikpati gratefully acknowledges CSIR for the financial support in the form of a fellowship (Award No. 9/79(248)/89-EMR-I,dt,20.10.89). We wish to thank the referee of the paper, Dr. P. Ulmschneider, for his helpful comments.

REFERENCES

Choudhuri, A. R., Auffret, H., & Priest, E. R. 1992, Sol. Phys., 143, 49 (Paper I)
Fontenla, J. M., Avrett, E. H., & Loeser, R. 1990, ApJ, 355, 700
Hollweg, J. V. 1981, Sol. Phys., 70, 25
———. 1982, ApJ, 257, 345
———. 1984, ApJ, 277, 392
———. 1990, Comp. Phys. Rep., 122, 205
Lamb, H. 1932, Hydrodynamics (Cambridge: Cambridge Univ. Press)
Narain, U., & Ulmschneider, P. 1990, Space Sci. Rev., 54, 377
Parker, E. N. 1986, in Coronal and Prominence Plasmas, ed. A. I. Poland (NASA Conf. Publ. 2442), 9
Priest, E. R. 1982, Solar Magnetohydrodynamics (Dordrecht: Reidel)
Rae, I. C., & Roberts, B. 1982, ApJ, 256, 761
Roberts, B. 1985, in Solar System Magnetic Fields, ed. E. R. Priest (Dordrecht: Reidel), 37
Spruit, H. C. 1981, A&A, 98, 155
———. 1984, in Small Scale Dynamical Processes in Quiet Stellar Atmosphere, ed. S. L. Keil (Sunspot, NM: National Solar Observatory), 249
Ulmschneider, P., Priest, E. R., & Rosner, R. 1991, Mechanisms of Chromospheric and Coronal Heating (Berlin: Springer-Verlag)
Vernazza, J. E., Avrett, E. H., & Loeser, R. 1981, ApJS, 45, 635
Vigneau, J., Roudier, R., Muller, R., & Auffret, H. 1992, preprint
Zugzda, Y. D., & Locans, M. 1982, Sol. Phys., 76, 77